Microsyst Technol (2016) 22:1163–1171
DOI 10.1007/s00542-015-2688-z

TECHNICAL PAPER

A CMOS-MEMS IR device based on double-layer thermocouples

Cheng Lei[1,2] · Haiyang Mao[2,3] · Wen Ou[2,3] · Chenyang Xue[1] · Licheng Tang[1,2] · Tao Yang[2,3] · Dapeng Chen[2,3] · Jijun Xiong[1]

Received: 28 June 2015 / Accepted: 23 September 2015 / Published online: 5 October 2015

Abstract In this work, a thermopile-based MEMS IR sensor is reported. In the device, a double-layer thermocouple strip structure and thermal-conductive-electrical-isolated structures are adopted thus to reduce the size and to improve performance of the whole device. After being packed into a TO-5 package, the sensor achieves a responsivity of 1151.14 V/W, a detectivity of 4.15 × 10^8 cm $Hz^{1/2}$/W, and a response time of 14.46 ms. Besides, in measurements of varied temperatures and vacuum pressures, the thermopile proposed in this work could reach relatively high sensitivities. This indicates that such a device can also function as a temperature sensor and a vacuum sensor. In this way, the applications of thermopiles are broadened.

1 Introduction

Infrared (IR) detectors have been widely used in both military and civilian fields, the applications include missile guidance, military security systems, thermograph, night-vision equipments, gas analysis devices, and others (Mattsson et al. 2009; Frank and Meixner 2001; Mao et al. 2013). Thermopile IR detectors based on Seebeck principle are one type of the most important IR devices, as they need neither cooling systems, nor alternative radiation controllers, besides, they are well adapted to both dynamic and static testing systems (Li et al. 2010; Schieferdecker et al. 1995).

Currently, thermopile devices composed of different thermoelectric materials have been reported. In these devices, thermo-electric materials such as Bi_2Te_3 and Sb_2Te_3 are favored ascribed to their large figure-of-merit, Z_T, consequently, high performance can be obtained from this type of IR devices (Goncalves et al. 2006; Shea et al. 2014; Zou et al. 2002). However, the thermo-electric materials used in these conventional thermopiles are not compatible with complementary metal oxide semiconductor (CMOS) fabrication, thus mass preparation and low cost can hardly be achieved (Xie et al. 2010). To solve this problem, MEMS thermopiles composed of materials like Poly-Si and Al have been presented, such devices can be fabricated by using CMOS-compatible processes. However, in these IR sensors, the thermocouples are usually distributed in a single layer (Wang et al. 2010; Calaza et al. 2006), namely, structures of single-layer thermocouple strips (SLTS) are adopted in conventional IR devices. As a result, the sizes of the devices cannot be effectively scaled-down, and the number of the thermocouple strips is limited. Consequently, the performance can only reach a relatively low level. Meanwhile, in structures of thermopile-based devices, the hot junctions overlap the IR absorber area usually with a layer of thermal-isolation material, which as a result, decreases the heat delivered from the IR absorber to the hot junctions. At the same time, the device substrate usually functions as a heat-sink, similarly, cold junctions overlap the substrate with another thermal-isolation layer between them, thus the temperatures of the cold junctions and the substrate cannot be the same.

✉ Jijun Xiong
xiongjijunnuc@126.com

1 National Key Laboratory for Electronic Measurement Technology, North University of China, Taiyuan 030051, People's Republic of China

2 Smart Sensing R&D Center, Institute of Microelectronics, Chinese Academy of Sciences, Beijing 100029, People's Republic of China

3 Smart Sensor Engineering Center, Jiangsu R&D Center for Internet of Things, Wuxi 214135, People's Republic of China

In this paper, a MEMS thermopile-based IR sensor with high performance is presented. In the sensor, a structure of double-layer thermocouple strips (DLTS) is adopted, thus the dimension of the sensor is almost reduced to half of the SLTS structures, and meanwhile, more thermocouple strips can be integrated into the sensor. Besides, N-type and P-type Poly-Si are adopted as the thermo-electric materials for the DLTS. Compared with Al/N-type Poly-Si and Al/P-type Poly-Si, the N-type and P-type Poly-Si materials present a larger difference in Seebeck coefficients and smaller thermal conductance (Xie et al. 2011). Moreover, such materials are commonly used in micro-fabrication, thus the preparation process for the whole devices can be fully CMOS-compatible. Consequently, mass preparation, low cost and high performance becomes practical. Furthermore, thermal-conductive-electrical-isolated (TCEI) structures, with a relatively large thermal conductivity and a small electrical conductivity, are adopted both under the cold junctions and the hot junctions, thus the temperatures can be kept in consistence between the hot junctions and the IR absorber as well as between the cold junctions and the substrate. Therefore, higher temperature difference between the cold junctions and the hot junctions is achieved, leading to higher performance in IR detection. In addition, measurements of the thermopile device at different temperature and different vacuum pressures were performed, which demonstrate that the IR sensor presented herein can also function as a temperature sensor and a vacuum sensor.

2 Structural design

2.1 Theory of thermopile

Thermopile is an electronic component which converts thermal information into electrical signals, it is made of thermocouple strips electrically connected in series. A thermocouple is also a thermoelectric conversion sensor composed of two materials with different Seebeck coefficients. The ends of the two materials form hot junctions and cold junctions, respectively, and the two types of materials contact with each other at one of the junctions. When the hot junctions are heated, according to Seebeck effect, a thermoelectric potential can be generated at the cold junctions. Herein, the junctions exposed to higher temperature are called "hot junctions", similarly, so called "cold junctions" are the spots exposed to lower temperature. The thermopile detector is an array of thermocouple, thus a higher output signal can be obtained. Herein, thermocouple strips are supported on a floating thin dielectric layer with their hot junctions connected to the absorber area and the cold junctions located on the silicon heat-sink. Here, temperature of the heat-sink is kept consistent with the ambience. That is to say, when there is IR radiation, a temperature difference T_{diff} will be generated between the hot junctions and the cold junctions. According to the Seebeck effect, the thermopile will acquire an electrical output voltage ΔU without any applied voltage bias. The output voltage of the thermopile can be described mathematically as (Escriba et al. 2005; Wang et al. 2009)

$$\Delta U = NT_{\text{diff}}(\alpha_1 - \alpha_2) = NT_{\text{diff}}\alpha \quad (1)$$

where N is the number of thermocouple strips, α_1 and α_2 refer to the Seebeck coefficients (μV/K) of the two materials, and α is the difference between α_1 and α_2.

Responsivity, detectivity and response time are the main parameters to characterize performance of a thermopile IR detector. The responsivity (V/W) of the device can be obtained by (Escriba et al. 2005)

$$R_{\text{v}} = \frac{\Delta U}{P_0} = \frac{\Delta U}{\varphi_0 A_{\text{d}}} \quad (2)$$

where, P_0 is the radiative power, φ_0 is the power density of the IR radiation, A_{d} is the area of the absorber. According to the Stefan–Boltzmann law, the radiation power density from the IR source over the thermopile is (under the assumption of $T_{\text{diff}} \ll T_0$)

$$\varphi_0 = \frac{C_{\text{r}} \cdot \sigma \cdot \varepsilon_1 \cdot (T_1^4 - T_0^4)}{A_{\text{s}} \cdot \pi \cdot d_0^2} \quad (3)$$

where C_{r} is root-mean-square (RMS) conversion factor of the chopper, ε_1 is the black degree of the IR source, σ is the Stefan–Boltzmann constant, T_1 is the temperature of the IR source, T_0 is the ambient temperature, A_{s} is the radiation area of the IR source, and d_0 is the distance between the IR source and the thermopile device. When contributions of the Joule heat and Peltier effect are neglected, the T_{diff} can be presented as

$$T_{\text{diff}} = \frac{R_{\text{L}}}{R_{\text{L}} + R_{\text{H}} + R_{\text{C}}} \Delta T \quad (4)$$

where R_{L} is the thermal resistance between hot junctions and cold junctions, R_{H} is the contact thermal resistance between absorber area and hot junctions, R_{C} is the contact thermal resistance between silicon heat-sink and cold junctions. ΔT is the temperature difference between absorber and the heat-sink, which can be determined by (Escriba et al. 2005)

$$\Delta T = \eta \cdot P_0 \cdot R_{\text{th}} \quad (5)$$

where η is the absorption rate of the absorber, and R_{th} is the total thermal resistance of the thermopile. According to energy conservation law, when the absorber is irradiated by IR light, the absorber converts incident IR radiation energy into heat Q_{absorb} which will be transferred through three different types of thermal resistance: thermal resistance of the structure R_s, thermal resistance of the atmosphere air R_g and thermal resistance of the radiation R_r. Therefore, the multiplicative inverse of total thermal resistance of the thermopile can be calculated by (Xu et al. 2009)

$$\frac{1}{R_{th}} = \frac{1}{R_s} + \frac{1}{R_g} + \frac{1}{R_r}. \tag{6}$$

Herein, R_s consists of R_L, R_H and R_C, thus the thermal resistance of the structure can be described as

$$R_s = R_L + R_H + R_C. \tag{7}$$

Further, the responsivity of the device can be calculated by

$$R_v = \frac{\eta N \alpha R_{th} R_L}{R_s} \tag{8}$$

where R_L can be expressed as (Du and Lee 2002)

$$R_L = \frac{1}{\sum_{i=1}^{4} N \frac{\lambda_i \cdot d_i \cdot w_i}{l_i}}. \tag{9}$$

Herein, λ_i, w_i, d_i, l_i are the thermal conductivity, width, thickness and length of each thermocouple strip (i = 1 for the P-type thermocouple strips; i = 2 for the N-type thermocouple strips; i = 3 for the isolation layer; i = 4 for supporting membrane).

Besides, the thermal conductance resulted from heat conduction of air is (Hsun and Chengkuo 1999)

$$G_g = \lambda_g (A_d + A_p) \left(\frac{1}{d_1} + \frac{1}{d_2} \right) = \frac{1}{R_g} \tag{10}$$

where λ_g is the thermal conductivity of the atmosphere air, A_p is the whole area of thermocouple strips, d_1 is the distance between the membrane and the bottom of heat insulation cavity, d_2 *is* the distance between the membrane and the package cap.

Meanwhile, the thermal conductance resulted from radiation is under the assumption of $T_{diff} \ll T_0$ (Graf et al. 2007), and there is

$$G_r = 4 A_d \varepsilon_2 \sigma T_0^3 = \frac{1}{R_r} \tag{11}$$

where ε_2 is the effective emissivity of the absorber. Therefore, we can also calculate the responsivity as

$$R_v = \frac{\eta N \alpha R_L}{1 + (G_g + G_r)(R_L + R_H + R_C)}. \tag{12}$$

Consequently, the detectivity of the device can be determined by (Escriba et al. 2005)

$$D^* = \frac{R_v \sqrt{A_d \Delta f}}{U_n} \tag{13}$$

where Δf is the measurement frequency bandwidth and U_n is the noise voltage of the thermopile, where U_n is dominated as Johnson noise, which can be written as

$$U_n = \sqrt{4 k R_0 T_0 \Delta f} \tag{14}$$

where k is the Boltzmann constant, R_0 is the electrical resistance of the thermopile strips. Then the detectivity can be calculated as

$$D^* = R_v \sqrt{\frac{A_d}{4 k T_0 R_0}}. \tag{15}$$

Another important parameter is the response time (τ), which is expressed as

$$\tau = C_{th} \cdot R_{th} \tag{16}$$

where C_{th} is the total thermal capacitance of the thermopile which consists of two parts, C_{ab} and C_s. Herein, C_{ab} is the thermal capacitance of the absorber and C_s is the thermal capacitance of the thermocouple region

$$C_{th} = C_{ab} + C_s. \tag{17}$$

Then we can also calculate the C_{th} as

$$C_{th} = \sum_{j=1}^{6} \left[(A_d \cdot d_j \cdot \rho_j \cdot c_j) + (l_j \cdot w_j \cdot d_j \cdot \rho_j \cdot c_j) \right] \tag{18}$$

where l_j, w_j, d_j, ρ_j, c_j are the length, width, thickness, mass density and specific heat of each part (j = 1 for the absorber, j = 2 for the supporting membrane of the absorber, j = 3 for the P-type thermocouple stripes; j = 4 for the N-type thermocouple strips; j = 5 for the isolation layer; and j = 6 for the supporting membrane).

2.2 Design of thermopile

As demonstrated in Sect. 2.1, optimized thermo-electric materials for high-performance thermopile devices should be with small thermal conductance, low electrical resistance and high Seebeck coefficient difference. As is restricted by the CMOS compatibility, only few materials like N-type and P-type Poly-Si, Al and N/P doped Poly-Si can meet the requirements. Thermoelectric properties of related materials are shown in Table 1, from which we can see that the Seebeck coefficient difference between Al and N/P doped Poly-Si is much smaller than that between N-type and P-type Poly-Si. Moreover, thermal conductance of Al is much larger than that of the N-type and P-type Poly-Si. As described in Eqs. (1), (12) and (15), lower

Seebeck coefficient difference and higher thermal conductance will reduce the performance of the thermopile. Taking all the factors into consideration, N-type and P-type Poly-Si are chosen to construct the thermocouple strips.

In order to further scale-down sizes of the thermopile devices while maintaining their high performance, a thermopile based on Poly-Si and DLTS structure is presented. Figures 1 and 2 schematically display a conventional SLTS structure (Fig. 1) and the DLTS one (Fig. 2) we proposed. As illustrated in Fig. 1, the thermocouple strips are distributed symmetrically along the longer sides of a rectangular absorber. The hot junctions overlap the absorber and the cold junctions overlap the heat-sink both over thermal-isolation structures. The N- or P-type Poly-Si thermocouple strips and the aluminum thermocouple strips are all connected in series by a metallic layer to form a thermopile,and all the thermocouple strips are typically fabricated on the same layer. Similarly, the thermocouple strips in a DLTS-based device (Fig. 2) are also distributed symmetrically along the longer sides of a rectangular absorber. However, the hot junctions overlap the absorber and the cold junctions overlap the heat-sink both over TCEI structures. The P-type Poly-Si thermocouple strips and the N-type Poly-Si thermocouple strips are adopted to form a thermopile, and

Table 1 Thermo-electric properties of various materials used in theoretical calculations (Allison et al. 2003; McConnell et al. 2001; Strassera et al. 2004)

Materials	Al	N-type Poly-Si (doped @ 3.64E20 cm^{-3})	P-type Poly-Si (doped @ 1.82E20 cm^{-3})	SiO_2	SiN_x
Seebeck coefficient (μVK^{-1})	−1.66	−124.17	105.76	–	–
Thermal conductivity (Wm^{-1}K^{-1})	237	35	30	1.2	16.7
Resistivity (μ Ω m)	0.03	2.7	6.55	–	–

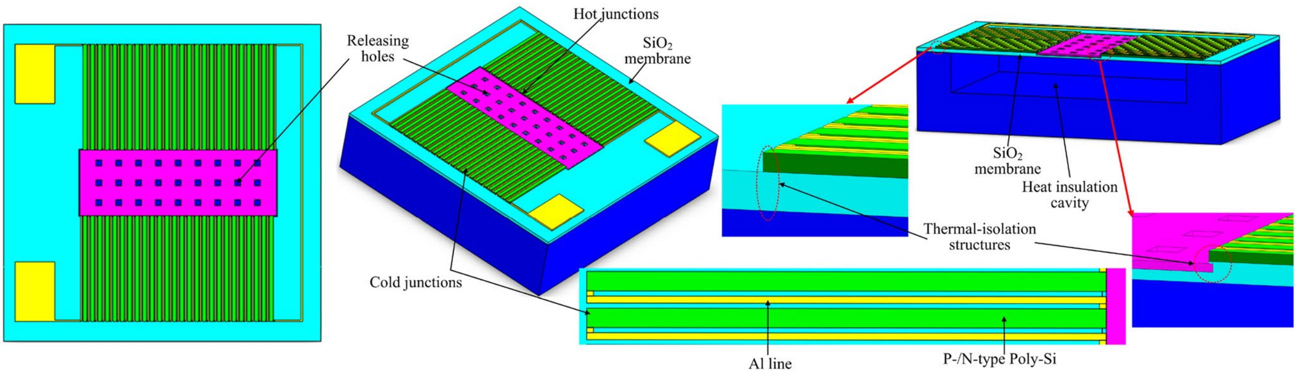

Fig. 1 Schematic diagrams of a SLTS thermopile

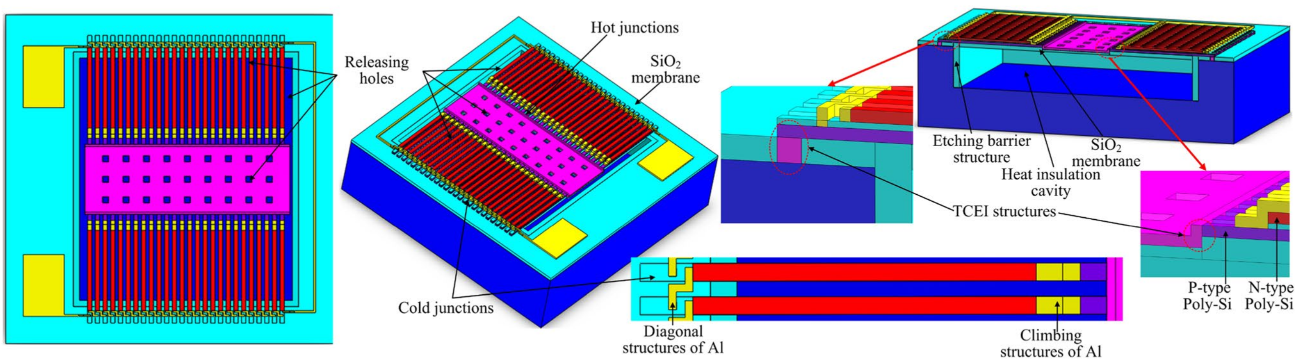

Fig. 2 Schematic diagrams of a DLTS thermopile

Table 2 Parameters of the thermopile device presented in this work

	N-type Poly-Si	P-type Poly-Si	SiO_2 electrical isolation layer	Absorber area
Size (L × W×H)	183 × 5×0.55 μm^3	198 × 5×0.55 μm^3	0.4 μm (H)	500 × 200 μm^2 (L × W)
Number	96	96	96	1

the different types of strips are located on two different layers. At the hot junctions, the N-type and P-type strips are connected using climbing structures of Al. Similarly, they are crossly linked at the cold junctions by diagonal structures of Al. Compared with the SLTS device, the DLTS-based ones exhibit higher responsitivity and detectivity. According to Eq. (12), R_v of the SLTS thermopile is no larger than half of that of the DLTS device. Meanwhile, the D^* of DSTL thermopile is higher than that of SLTS thermopile, according to Eq. (15). Besides, according to Eqs. (9) and (12), structural size of the DLTS thermopiles may be further scaled down by reducing the length of the thermocouple strips (at the expense of reducing thermal resistance), thus to maintain relatively higher performance when compared with the SLTS thermopiles.

In thermopile-based devices, a layer of thermal-isolation material between the absorber and the hot junctions often causes high contact thermal resistances. Similar problems also occur between the heat-sink and the cold junctions. According to Eqs. (1), (4) and (12), such high contact thermal resistances would limit the performance of the thermopile sensors. In addition, recent CMOS-compatible micromachined thermopiles usually adopt XeF_2 to release the structures. However, such an isotropic etching step from the front-side would easily lead to excessive release, as a result, the cold junctions and the electrodes might be floated to damage.

In order to avoid these drawbacks, the absorber and the P-type strips are connected at the hot junctions with TCEI structures, meanwhile, at the cold junctions, TCEI structures are also used to connect the P-type strips to the heat-sink. Herein, each of the TCEI structure consists of a SiN_x layer, compared with a silicon dioxide layer, the nitride one is thermally conductive and electrically isolated. In addition, etching barrier structures are integrated in our device to prevent floating of the cold junctions and the electrodes in case of excessive release. With all these efforts, it is expected that the performance of the thermopile devices can be improved.

Structural parameters of our thermopile device are described in Table 2, based on these parameters, performances of the device are theoretically calculated. The results demonstrate that responsivity of the device reaches 255.83 V/W, detectivity reaches 2.54E8 cm $Hz^{1/2}$/W, and time constant reaches 13.09 ms.

3 Fabrication

The fabrication process of the thermopile device is shown in Fig. 3. In order to realize the etching barrier structures, firstly, a ring-shaped deep trench is formed by using deep reactive ion etching, then the trench is filled with thermal SiO_2 and Tetraethylorthosilicate (TEOS) deposited by using a low pressure chemical vapor deposition (LPCVD) process. After reverse etching of the thermal SiO_2 and the TEOS layers, the wafer surface is thermally oxidized. In our experiment, the thickness of the silicon oxide layer was 8000 Å (Fig. 3a), and this layer will further function as a supporter for the thermocouple strips and the absorber. Then, a SiN_x layer is deposited and photo-patterned to fill the windows in the SiO_2 layer opened at positions of the cold junctions, and these SiN_x blocks will further be used as TCEI structures (Fig. 3b). Then, Poly-Si and SiO_2 layers are deposited alternatively over the wafer, where the two Poly-Si layers with the same thickness (which was 5500 Å in our experiment) are P- and N-doped. Besides, the SiO_2 layer between the two Poly-Si films plays the role as an isolator, which was 4000 Å thick (Fig. 3c). Later on, the three layers are photo-patterned, thus a DLTS structure is formed (Fig. 3d). Herein, the P-type Poly-Si located at the lower layer was implanted with B^+, using 10^{16} cm^{-2} as the doping dose and 65 keV as the energy. Similarly, the N-type Poly-Si was implanted with P^- of 2×10^{16} cm^{-2} @ 80 keV.

After that, a protecting layer is deposited over the DLTS structure, and Al is patterned on the protecting layer to connect the thermocouple strips into a series. Then, a passivation layer (4000 Å SiO_2) is deposited on the thermocouples by plasma enhanced chemical vapor deposition (PECVD) (Fig. 3e). Subsequently, the SiO_2 layer over the P-type strips at the ends of the hot junctions is removed, thus part of the P-type strips is revealed. Following that, a SiN_x film (with thickness of ~6000 Å) is deposited on the SiO_2 layer and patterned into the absorber. Herein, the SiNx at the absorber edges covers the revealed hot junction ends of the P-type strips, in this way, heat loss at the hot junctions can be reduced (Fig. 3f). Later on, a SiO_2 dielectric layer is further deposited by PECVD, and then, releasing windows are opened in this layer (Fig. 3g). Finally, the thermopile device is released by isotropic etching of XeF_2 gas (Fig. 3h). The fabricated thermopile devices are shown in Fig. 4, where an SEM image of the structure is exhibited in Fig. 4a, photos of a chip before and after TO packing are demonstrated in Fig. 4b, c.

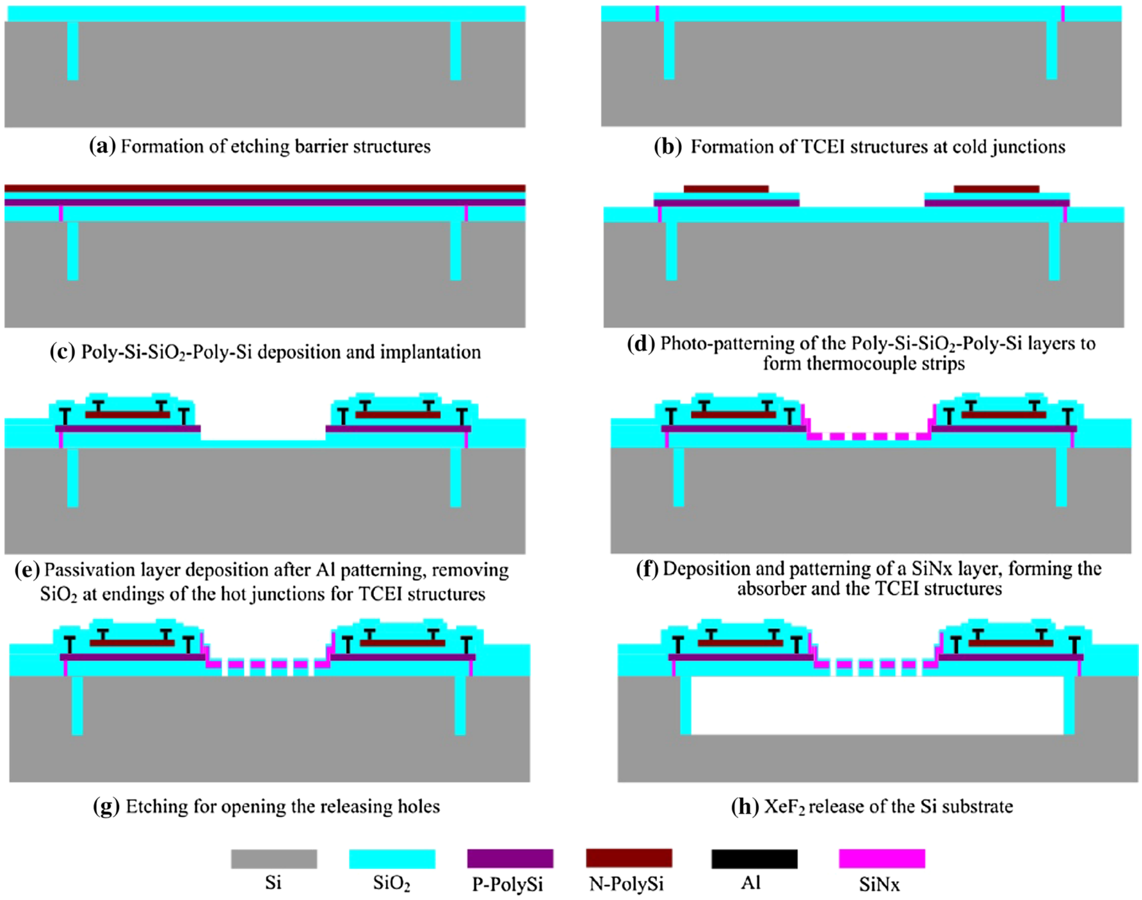

Fig. 3 Fabrication process of the thermopile device

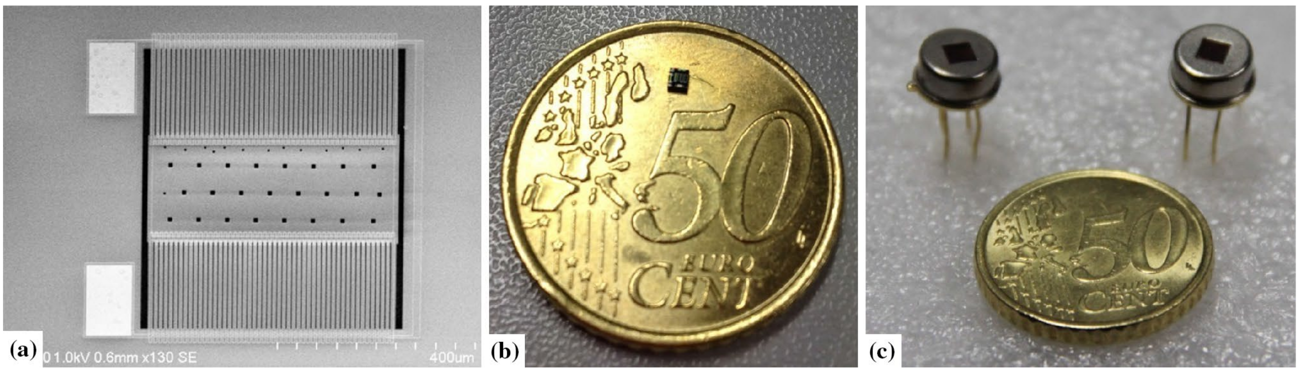

Fig. 4 Images of the thermopile devices, **a** SEM of the structure, **b** unpacked and **c** TO-5 packed thermopile devices

4 Measurement and discussion

4.1 IR radiation sensing

In order to characterize IR radiation performance of the detector, a measurement system as shown in Fig. 5 was set up. In the measurement, the detector was installed within a cooling system, which was used to maintain temperature of the heat-sink (as well as the cold junctions) to be consistent with ambient temperature (22 °C @ 36 % RH). Then, the detector and the cooling system were placed in front of a blackbody, with a fixed distance between the blackbody and the detector. In such a case, the power density of the

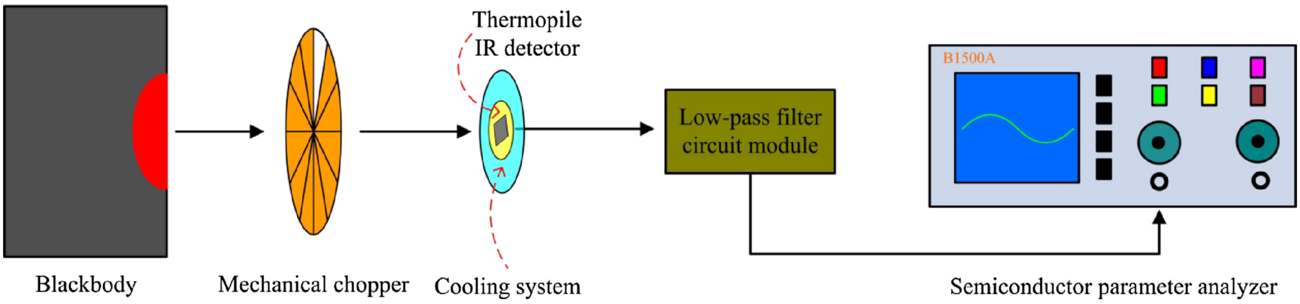

Fig. 5 Schematic measurement system for IR radiation detection

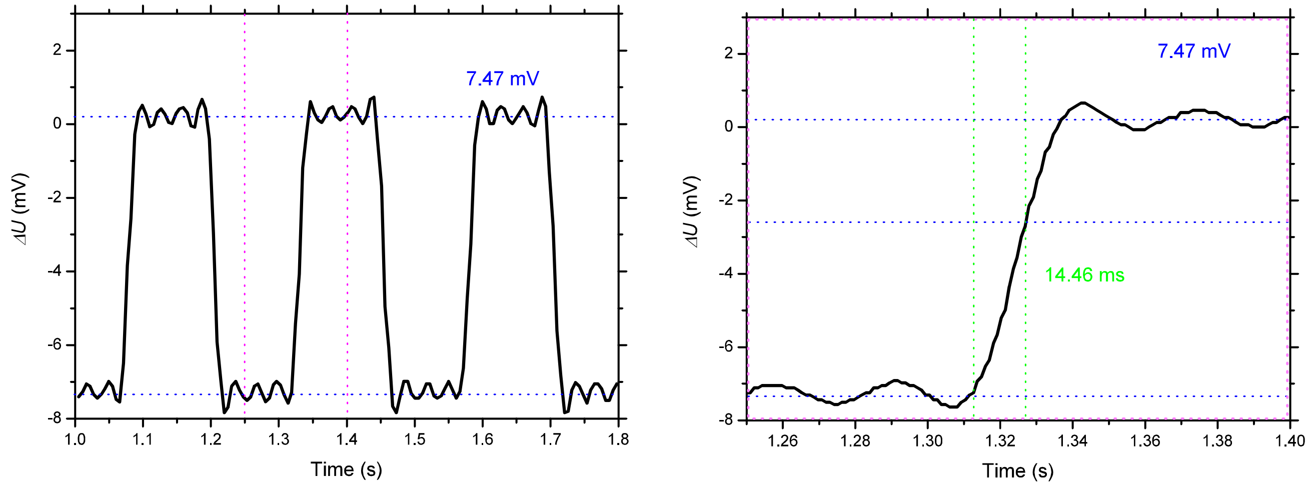

(a) Output voltage signal with several cycles

(b) Output voltage within a rising edge

Fig. 6 Output signals of a thermopile IR detector at 4 Hz and 500 K

applied IR radiation on the detector surface could reach a desirable value. Besides, in this system, a mechanical chopper was used to control the chopping frequency, a low-pass filter circuit module was devoted to avoiding noise with high frequency and a semiconductor parameter analyzer was utilized to output the signals.

In our IR radiation detection, the distance between the blackbody and the detector was 90 mm, the temperature of the blackbody was set to be 500 K, and frequency of the mechanical chopper was set at 4 Hz. With such settings, the power density on the detector surface was 66.73 W/m^2. The output voltage signals of the thermopile device are illustrated in Fig. 6, where Fig. 6a shows the response voltage with several cycles, and a cycle period of 250 ms and amplitude of 7.47 mV can be observed. To obtain response time of the device, a rising edge of the signal in one of the cycles is magnified, and the time required to reach 63 % of the maximum voltage is acquired as the time constant, which is 14.46 ms (shown in Fig. 6b). Herein, the electrical resistance R_0 of the thermopile strips is 458.5 KΩ.

Based on the theories discussed in Sect. 2.1, performance of the IR thermopile detector can be calculated.

The responsivity R_v calculated from the response voltage amplitude by using Eq. (2) is 1151.14 V/W. Similarly, the detectivity D^* reaches 4.15 × 10^8 cm Hz$^{1/2}$/W according to Eq. (15). Herein, the values of R_v and D^* are relatively larger than the theoretically calculated ones due to overvalued doping concentrations in the implantation processes. Since in practical implantation, the actual projected ranges might reach a distance beyond the central line of the Poly-Si layers, therefore, the doping concentrations might be smaller than the theoretical ones, thus the Seebeck coefficients are enhanced (Allison et al. 2003), and at the same time, the electric resistance R_0 is also enlarged. Because of the growth in R_0, the D^* could not reach a very high increase as that of R_v.

4.2 Temperature sensing

In order to characterize its ability for temperature sensing, an unpacked thermopile chip was placed in a chamber, in

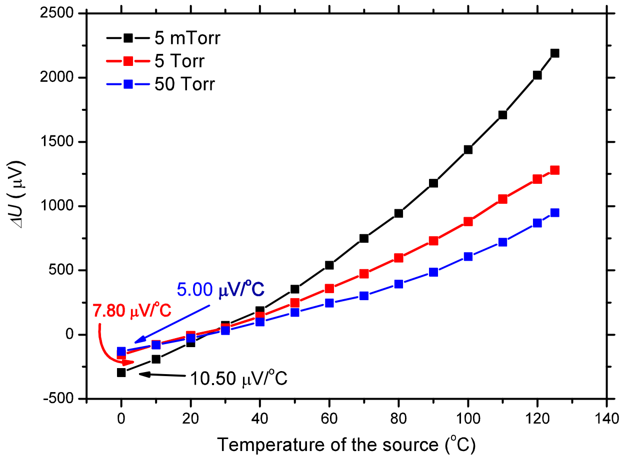

Fig. 7 Output of the thermopile device at different temperatures

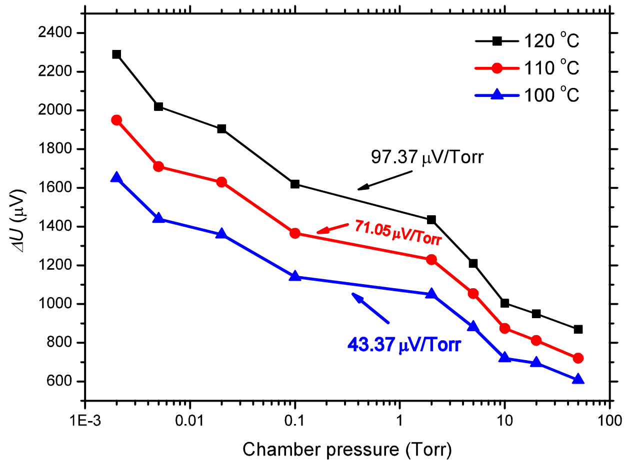

Fig. 8 Output of the thermopile device at different vacuum pressures

which the temperature and vacuum pressure can be precisely controlled. At the same time, the measurement system was also equipped with a probe station, a blackbody and an analyzer B1500A. The probes were connected with the metallic Pads in the device, and the blackbody was used to provide heat in the chamber. Once the device sensed the temperature variations, its output voltages would alter and thus the signals delivered to the B1500A could be varied. As the power density of IR radiation on the detector surface varied because of the blackbody temperature changing, according to Eqs. (1), (2), (4) and (5), the output voltage changed. In the measurement system, the temperature variations were provided by a surface blackbody and the distance between the blackbody and the thermopile chip was 150 mm. In the measurement, the temperature of IR source was varied from 0 to 125 °C, while the vacuum pressures were kept at constant values like 5 mTorr, 5 and 50 Torr. Then, the output voltages of the thermopile chip were captured by the B1500A. As shown in Fig. 7, the output voltages increase when the temperature is changed from 0 to 125 °C. The sensitivities of the device at 5 mTorr, 5 and 50 Torr reach 10.50, 7.80 and 5.00 μV/°C, respectively. Accordingly, the thermopile can have potential applications in indirect measurement of temperature and can function as a temperature sensor.

4.3 Vacuum pressure sensing

Similarly, another packed thermopile chip was placed in the same chamber described above so as to characterize its ability of vacuum pressure sensing. In addition to the aforementioned system, in this measurement, a vacuum pump was used to provide vacuum conditions for the chamber. When the gas pressure is below certain limit, the heat transfer by a gas is proportional to the number of molecules (and hence to the pressure) transferring the heat and thermal conductivity of air starts to increase with increase of pressure (Sun et al. 2013). Herein, once the pressure in the chamber was changed, the device could sense the change, and thus its output voltages would alter and thus the signals delivered to the B1500A could be varied. At certain temperature (e.g. 120, 110 and 100 °C), the output voltages of the thermopile chip in response to different vacuum pressure were measured and the results are shown in Fig. 8. As shown in this figure, the output voltages decrease with the gradual increase of vacuum pressures. Herein, the pressure sensitivities of the device at 120, 110 and 100 °C reach 91.37, 71.05 and 47.37 μV/Torr. In light of this, thermopiles can be used as a vacuum gauge.

5 Conclusion

In this work, a DLTS-based IR device is designed and fabricated using a CMOS-compatible process. Theoretical analysis suggests that the DLTS device has advantages over a SLTS device in aspects of responsivity, detectivity as well as in size-control. With the usage of TCEI structures at the cold junctions and the hot junctions, the performances of the DLTS devices are further improved. Preliminary measurement results demonstrate that the DLTS-based IR device achieves a responsivity of 1151.15 V/W, a detectivity of 4.15 × 10^8 cm $Hz^{1/2}$/W, and a time constant of 14.46 ms. Moreover, such a DLTS-based IR device can also function as a temperature sensor and a vacuum sensor with high sensitivities.

Acknowledgments This work was supported by National Natural Science Foundation of China (Grant No. 61401458, 61335008, 61136006 & 51205373), Jiangsu Natural Science Foundation (Grant No. BK20131098), and Henan Province Collaborative Projects in Science and Technology (132106000073).

References

Allison SC, Smith RL, Howard DW, Gonzalez C, Collins SD (2003) A bulk micromachined silicon thermopile with high sensitivity. Sens Actuators A 104:32–39. doi:10.1016/S0924-4247(02)00478-8

Calaza C et al (2006) An uncooled infrared focal plane array for low-cost applications fabricated with standard CMOS technology. Sens Actuators A 132:129–138. doi:10.1016/j.sna.2006.04.027

Du C, Lee C (2002) Characterization of thermopile based on complementary metal-oxide semiconductor materials and post CMOS micromachining. Jpn J Appl Phys 41:4340–4345. doi:10.1143/JJAP.41.4340

Escriba C, Campo E, Esteve D, Fourniols JY (2005) Complete analytical modeling and analysis of micromachined thermoelectric uncooled IR sensors. Sens Actuators A 120:267–276. doi:10.1016/j.sna.2004.11.027

Frank J, Meixner H (2001) Sensor system for indoor air monitoring using semiconducting metal oxides and IR-absorption. Sens Actuator B 78:298–302. doi:10.1016/S0925-4005(01)00829-2

Goncalves L, Couto C, Alpuim P, Rowe D, Correia J (2006) Thermoelectric microstructures of Bi_2Te_3/$Sb_2Te_3$for a self-calibrated micro-pyrometer. Sens Actuators A 130–131:346–351. doi:10.1016/j.sna.2005.10.014

Graf A, Arndt M, Sauer M, Gerlach G (2007) Review of micromachined thermopiles for infrared detection. Meas Sci Technol 18:R57–R75. doi:10.1088/0957-0233/18/7/E01

Hsun D, Chengkuo L (1999) Optimization criteria of CMOS compatible thermopile sensors. SPIE 3893:116–126. doi:10.1117/12.368445

Li Y et al (2010) CMOS-compatible 8 × 2 thermopile array. Sens Actuators A 161:120–126. doi:10.1016/j.sna.2010.04.026

Mao H et al (2013) Fabrication of nanopillar forests with high infrared absorptance based on rough poly-Si and spacer technology. J Micromech Microeng 23:095033. doi:10.1088/0960-1317/23/9/095033

Mattsson C, Bertilsson K, Thungstrom G, Nilsson H, Martin H (2009) Thermal simulation and design optimization of a thermopile infrared detector with an SU-8 membrane. J Micromech Microeng 19:055016. doi:10.1088/0960-1317/19/5/055016

McConnell AD, Uma S, Goodson KE (2001) Thermal conductivity of doped polysilicon layers. J Microelectromech Syst 10:360–369. doi:10.1109/84.946782

Schieferdecker J, Quad R, Holzenkämpfer E, Schulze M (1995) Infrared thermopile sensors with high sensitivity and very low temperature coefficient. Sens Actuators A 46–47:422–427. doi:10.1016/0924-4247(94)00934-A

Shea R, Gawarikar A, Talghader J (2014) Process integration of co-sputtered bismuth telluride/antimony telluride thermoelectric junctions. J Microelectromech Syst 23:681–688. doi:10.1109/JMEMS.2013.2283795

Strassera M et al (2004) Micromachined CMOS thermoelectric generators as on-chip power supply. Sens Actuators A 114:362–370. doi:10.1016/j.sna.2003.11.039

Sun X et al (2013) A wide measurement pressure range CMOS-MEMS based integrated thermopile vacuum gauge with an XeF_2 dry-etching process. Sens Actuators A 201:428–433. doi:10.1016/j.sna.2013.07.020

Wang Z, Leonov V, Fiorini P, Hoof C (2009) Realization of a wearable miniaturized thermoelectric generator for human body applications. Sens Actuators A 156:95–102. doi:10.1016/j.sna.2009.02.028

Wang K et al (2010) Thermopile infrared detector with detectivity greater than 10^8 cm $Hz^{(1/2)}$/W. J Infrared Millim W 31:810–820. doi:10.1007/s10762-010-9635-y

Xie J, Lee C, Feng H (2010) Design, fabrication, and characterization of CMOS MEMS-based thermoelectric power generators. J Microelectromech Syst 19:317–324. doi:10.1109/JMEMS.2010.2041035

Xie J, Lee C, Wang M, Tsai J (2011) Microstructures for characterization of seebeck coefficient of doped polysilicon films. Microsyst Technol 17:77–83. doi:10.1007/s00542-010-1183-9

Xu D, Xiong B, Wang Y, Liu M, Li T (2009) Integrated micromachined thermopile IR detectors with an XeF_2 dry-etching process. J Micromech Microeng 19:125003. doi:10.1088/0960-1317/19/12/125003

Zou H, Rowe D, Williams S (2002) Peltier effect in a co-evaporated Sb_2Te_3(P)-Bi_2Te_3(N) thin film thermocouple. Thin Solid Films 408:270–274. doi:10.1016/S0040-6090(02)00077-9